Journal of Power Sources 192 (2009) 291–296

Contents lists available at ScienceDirect

Journal of Power Sources

journal homepage: www.elsevier.com/locate/jpowsour

Co-doped Sr_2FeNbO_6 as cathode materials for intermediate-temperature solid oxide fuel cells

Tian Xia [a,*], Nan Lin [a], Hui Zhao [a], Lihua Huo [a], Jingping Wang [b], Jean-Claude Grenier [c]

[a] School of Chemistry, Chemical Engineering and Materials, Heilongjiang University, Harbin 150080, People's Republic of China
[b] College of Materials Science and Chemical Engineering, Harbin Engineering University, Harbin 150001, People's Republic of China
[c] Institut de Chimie de la Matière Condensée de Bordeaux (ICMCB-CNRS), 33608 Pessac Cedex, France

ARTICLE INFO

Article history:
Received 5 February 2009
Received in revised form 10 March 2009
Accepted 11 March 2009
Available online 24 March 2009

Keywords:
Solid oxide fuel cells
$Sr_2Fe_{1-x}Co_xNbO_6$ cathode material
Electrochemical performance

ABSTRACT

$Sr_2Fe_{1-x}Co_xNbO_6$ ($0.1 \leq x \leq 0.9$) (SFCN) oxides with perovskite structure have been developed as the cathode materials for intermediate-temperature solid oxide fuel cells (IT-SOFCs). These materials are synthesized via solid-state reaction and characterized by XRD, SEM, electrical conductivity, AC impedance spectroscopy and DC polarization measurements. The reactivity tests show that the $Sr_2Fe_{1-x}Co_xNbO_6$ electrodes are chemically compatible with the $Zr_{0.85}Y_{0.15}O_{1.925}$ (YSZ) and $Ce_{1.9}Gd_{0.1}O_{1.95}$ (CGO) electrolytes at 1200 °C, and the electrode forms a good contact with the electrolyte after sintering at 1200 °C for 12 h. The total electrical conductivity that has a considerable effect on the electrode properties is determined in a temperature range from 200 °C to 800 °C. The highest conductivity of 5.7 S cm^{-1} is found for $Sr_2Fe_{0.1}Co_{0.9}NbO_6$ at 800 °C in air. The electrochemical performances of these cathode materials are studied using impedance spectroscopy at various temperatures and oxygen partial pressures. Two different kinds of reaction rate-limiting steps exist on the $Sr_2Fe_{0.1}Co_{0.9}NbO_6$ electrode, depending on the temperature. The $Sr_2Fe_{0.1}Co_{0.9}NbO_6$ electrode on CGO electrolyte exhibits a polarization resistance of 0.74 Ω cm^2 at 750 °C in air, which indicates that the $Sr_2Fe_{0.1}Co_{0.9}NbO_6$ electrode is a promising cathode material for IT-SOFCs.

1. Introduction

Solid oxide fuel cells (SOFCs) that convert directly chemical energy into electrical energy through electrochemical processes have been regarded as a promising energy conversion and generation system due to their high efficiency, fuel adaptability and low pollution [1,2]. An important consideration to both design and manufacturing research is the reduction of operating temperature in order to reduce production costs [3]. Making low cost intermediate-temperature solid oxide fuel cells (IT-SOFCs) supposes the operating temperature to be reduced down to 800 °C or lower. The improvement of cathode performance is one of the most important issues for the development of IT-SOFCs.

A number of investigations concerned with cathode materials are devoted to perovskite-type materials. Strontium doped lanthanum manganate $La_{1-x}Sr_xMnO_3$ (LSM), the earliest cathode material, is limited in use with respect to IT-SOFCs because of its low oxide-ion conductivity [4]. On the other hand, $La_{1-x}Sr_xCo_{1-y}Fe_yO_3$ (LSCF) with high oxide-ion conductivity has been extensively developed as cathode material in IT-SOFCs. However, it was reported that $La_{1-x}Sr_xCo_{1-y}Fe_yO_3$ has a relatively higher thermal expansion coefficient with respect to the use of the electrolyte [5,6]. $A_2BB'O_6$ oxides with the double-perovskite structure, which can accommodate large amounts of oxygen non-stoichiometry, have been previously known as tunneling magnetoresistance compounds [7]. Recently, studies on $Sr_2MgMoO_{6-\delta}$ have found that this material exhibits mixed ionic and electronic conducting property, much higher thermochemical stability and electrocatalytic activity [8–11]. Preliminary results are promising in terms of electrochemical performance and redox stability [9–11]. The majority of these investigations have been devoted to the Mg, Mn and Cr substituted materials due to their excellent anode performances [9]. Tao et al. prepared Sr_2FeNbO_6 and studied its structure, stability and electrical conductivity [12]. The results indicate that Sr_2FeNbO_6 has good thermochemical and structural stability over a wide range of oxygen partial pressures and that the thermal expansion coefficient is also compatible with most electrolyte materials [13]. This would lead to interesting engineering possibilities in terms of developing cathode materials for IT-SOFCs. In this paper, the perovskite structure oxides $Sr_2Fe_{1-x}Co_xNbO_6$ (SFCN) were synthesized and characterized. The suitability of SFCN as a cathode material based on $Zr_{0.85}Y_{0.15}O_{1.925}$ (YSZ) and $Ce_{1.9}Gd_{0.1}O_{1.95}$ (CGO) electrolytes was analyzed over the IT-SOFCs temperature range. The electrochemical performances of a SFCN cathode on CGO electrolyte were also investigated.

* Corresponding author. Tel.: +86 451 86608426; fax: +86 451 86608040.
E-mail address: xiatian0621@yahoo.com.cn (T. Xia).

0378-7753/$ – see front matter © 2009 Elsevier B.V. All rights reserved.
doi:10.1016/j.jpowsour.2009.03.025

2. Experimental

The single-phase $Sr_2Fe_{1-x}Co_xNbO_6$ ($0.1 \le x \le 0.9$) powders were prepared through solid-state reaction. Stoichiometric amount of $SrCO_3$ (≥99.5%), Fe_2O_3 (≥99.5%), Co_3O_4 (≥99.5%) and Nb_2O_5 (≥99.9%) was mixed and ground in an agate mortar, then calcined in air at 1300 °C for 24 h. The obtained materials were denoted as SFCN01 for $Sr_2Fe_{0.9}Co_{0.1}NbO_6$ and so on. YSZ (Tosoh, Japan) and CGO powders prepared according to Ref. [14] were pressed uniaxially at 200 MPa and sintered at 1400 °C for 12 h and 10 h to form dense pellets. The electrolyte pellets were about 1 mm in thickness and 11 mm in diameter.

The SFCN powders were mixed with terpineol to form ink, and subsequently painted on one side of the electrolyte pellet to form a working electrode (WE) with a surface area of 0.4 cm^2. Platinum paste was painted symmetrically on the other side of the pellet as the counter electrode (CE). A Pt wire was used as a reference electrode (RE) and put on the same side of the WE. Pt mesh attached to a Pt wire was used as the current collector. The cell was first heated at 500 °C to eliminate organic binders, then sintered at 1200 °C for 12 h in air.

The structure and phase purity of the materials were characterized by powder X-ray diffraction (XRD) using a Rigaku DMAX ΠB diffractometer with Cu Kα radiation. The morphology and microstructure of the sintered electrodes were observed with a Philips XL-30 field-emission scanning electron microscope (FE-SEM). The electrical conductivity of the materials was measured in air by the standard four-probe DC method on dense pellets. The as-prepared powders were pressed into the rectangular bars (2 mm × 2 mm × 25 mm) under a pressure of 150 MPa followed by sintering at 1300 °C for 12 h in air. The density of the sintered bars was measured by the Archimedes' method; it ranged between 85% and 90% of theoretical density. Pt leads were attached to the rectangular bar with Pt paste and fired at 800 °C for 1 h to obtain good electric contact.

AC impedance spectroscopy was carried out using an Autolab PGStat30 in the frequency range of 0.1 Hz to 1 MHz. The measurements were performed at an equilibrium potential as a function of temperature (550–800 °C) and oxygen partial pressure (N_2/O_2 mixed atmosphere). The DC polarization experiments were performed by the chronoampermetry method [15], which involved a potential step followed by recording the current density as a function of time. The cathode overpotential was calculated according to the following relation:

$$\eta_{WE} = \Delta U_{WR} - iR_{el}$$

where η_{WE} represents the cathode overpotential, ΔU_{WR} is the applied voltage between working electrode and reference electrode, i and R_{el} are the current flowing through the cell and the resistance of the electrolyte obtained from the impedance spectrum, respectively.

3. Results and discussions

Fig. 1A shows the XRD patterns of as-prepared SFCN powders. It is observed that all these materials crystallize in a single-phase perovskite structure; no impurities are detected. The XRD patterns of SFCN are indexed on a tetragonal unit cell, consistent with a structure related to Sr_2FeNbO_6 [12]. The reaction between electrode and electrolyte is undesirable for the long-term stability of SOFCs. The reactivity of $Sr_2Fe_{0.1}Co_{0.9}NbO_6$ (SFCN09) with YSZ and CGO electrolytes was studied by mixing thoroughly SFCN09 with YSZ or CGO in a 1:1 weight ratio, and then sintered at 1200 °C for 24 h. There are no new peaks identifiable or shift of XRD peaks in the patterns (Fig. 1B and C). Obviously the structures of SFCN09, YSZ

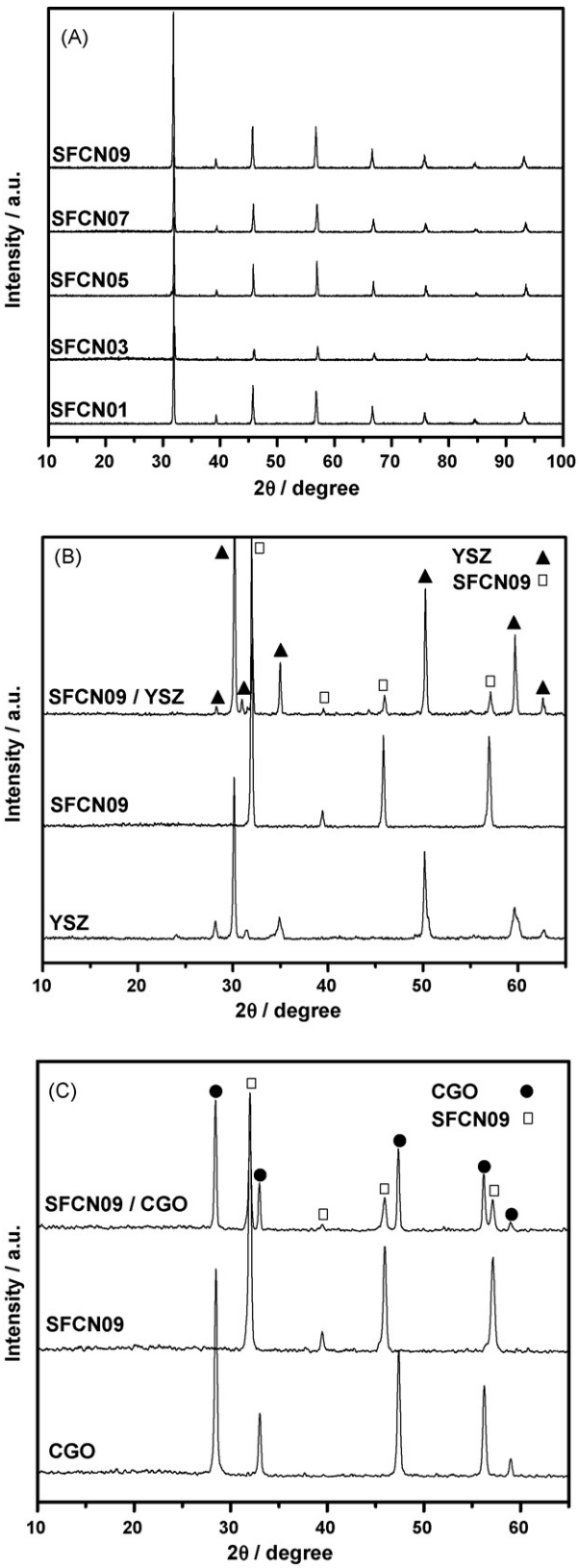

Fig. 1. The XRD patterns of (A) $Sr_2Fe_{1-x}Co_xNbO_6$ (SFCN) powders, (B) SFCN09, YSZ and SFCN09-YSZ mixture and (C) SFCN09, CGO and SFCN09-CGO mixture after heating at 1200 °C for 24 h in air.

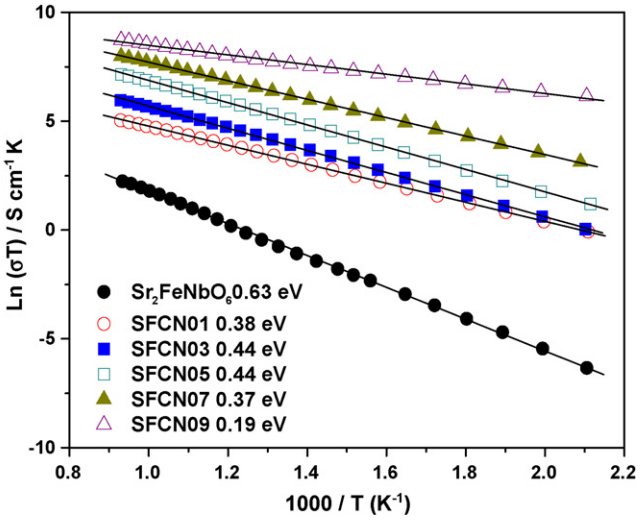

Fig. 2. Arrhenius plots of the electrical conductivity of $Sr_2Fe_{1-x}Co_xNbO_6$ (SFCN) measured in air.

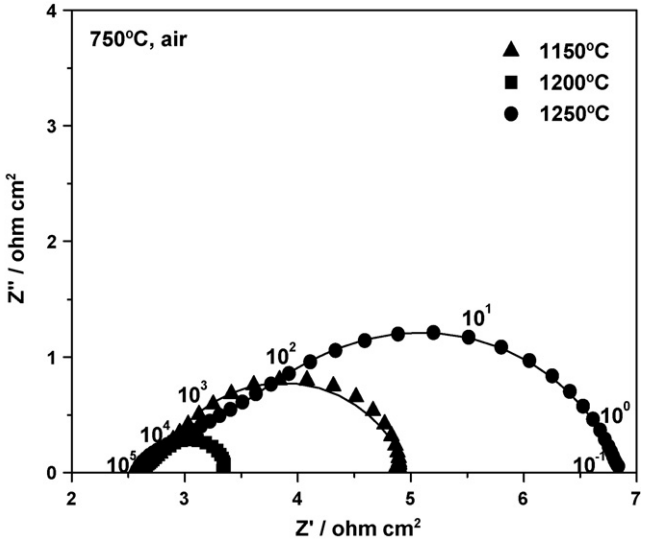

Fig. 3. Impedance spectra of the SFCN09 cathode on CGO electrolyte sintered at different temperatures for 12 h and then measured at 750 °C in air.

and CGO materials remain unchanged, indicating that there is no significant reaction between SFCN09 and electrolytes. For example, SFCN09 can be indexed on a tetragonal cell with lattice parameters of $a = 3.9716(2)$ Å and $c = 3.9812(4)$ Å, and CGO has a cubic ceria structure with lattice parameter of $a = 4.4211(1)$ Å. After calcining at 1200 °C, SFCN09 and CGO still remain their structures. The lattice parameters of SFCN09 and CGO are $a = 3.9721(1)$ Å, $c = 3.9816(2)$ Å and $a = 5.4214(5)$ Å, respectively. These results reveal that SFCN09 has a good chemical compatibility with the YSZ and CGO electrolytes. Additionally, the XRD pattern of YSZ shows the small peaks at $2\theta = 24°$, 28.5°, 31°, 34.5°, 50.5° and 60° in addition to pure cubic YSZ. These peaks suggest the presence of monoclinic and tetragonal YSZ, which might decrease the oxide-ion conductivity of electrolyte and further lower the electrode performance.

Arrhenius plots of the electrical conductivity of SFCN measured in air are shown in Fig. 2. The electrical conductivity of the SFCN oxides gradually increases with increasing temperature, indicating the thermally activated semiconductivity. The highest electrical conductivity is obtained for SFCN09 with a value of 5.7 S cm^{-1} at 800 °C. The total conductivity of SFCN increases with the increase of Co-doping, which can be assigned to the electron delocalization

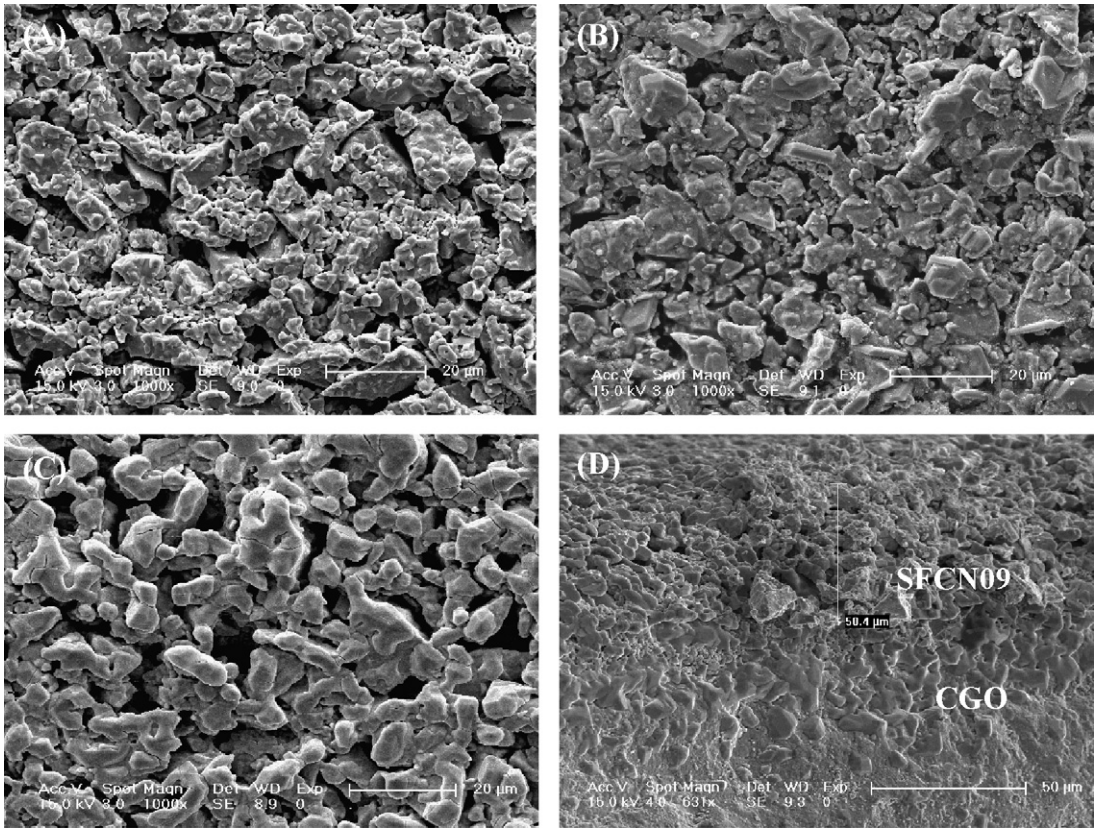

Fig. 4. FE-SEM images of the SFCN09/CGO cells sintered at 1150 °C (A); 1200 °C (B); 1250 °C (C); and the cross-section image of the test cell sintered at 1200 °C (D).

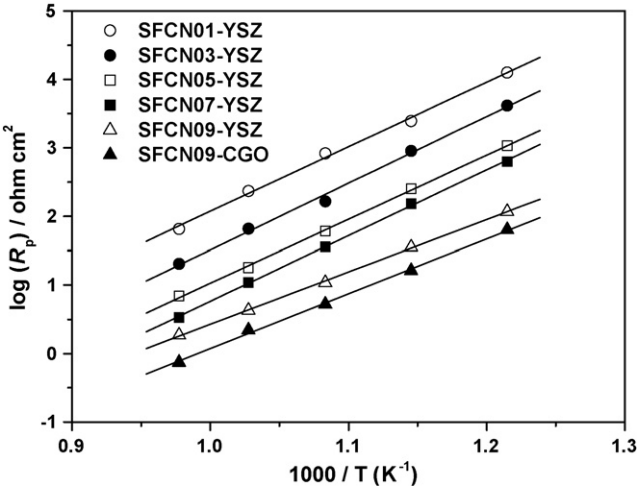

Fig. 5. Arrhenius plots of the polarization resistances of $Sr_2Fe_{1-x}Co_xNbO_6$ (SFCN) cathodes measured in air.

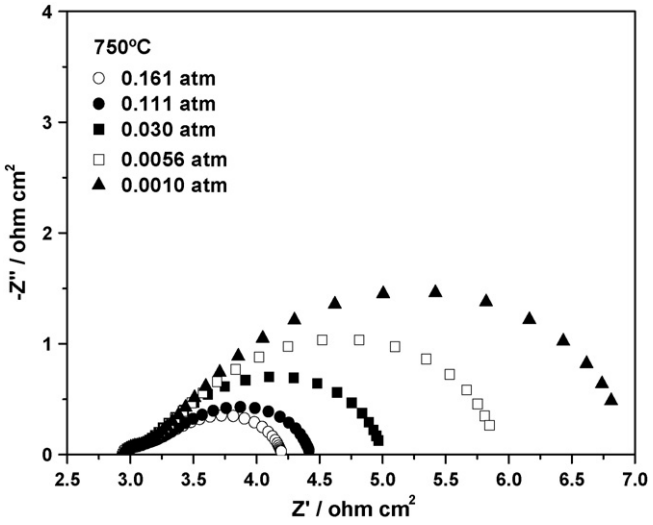

Fig. 6. Impedance spectra of the SFCN09/CGO cell measured at 750 °C under various oxygen partial pressures.

correlated to the stronger covalency of the Co–O bond compared to the Fe–O bond [16,17]. The activation energy of conductivity is determined from the plots and shown in Fig. 2.

In order to investigate the effect of sintering temperature on the SFCN cathode performances, different sintering conditions were studied. Fig. 3 shows the impedance spectra of the SFCN09 cathode on CGO electrolyte sintered at different temperatures for 12 h and then measured at 750 °C in air. The intercept value of the impedance arc with the real axis at high-frequency side corresponds to the resistance of the electrolyte and lead wires, while the value between the high-frequency *x*-axis and low-frequency one is attributed to the total polarization resistance (R_p) of the SFCN09 electrode. It is observed that R_p is relatively large when the sintering temperature is high (1250 °C). When the sintering temperature is 1200 °C, R_p reduces to the lowest value. R_p increases again when the sintering temperature is decreased down to 1150 °C. A similar result was obtained for SFCN09 electrode on YSZ electrolyte. It is well known that the sintering temperature has a dramatic effect on the electrode microstructure, which in turn will influence the electrode performances. Therefore, the microstructural evolution of the SFCN09 cathodes was further studied as a function of different sintering temperatures.

Typical FE-SEM images of SFCN09/CGO cells after sintering at different temperatures for 12 h are shown in Fig. 4. It can be seen that SFCN09 particles form poor contacts with each other when the sintering temperature is 1150 °C (Fig. 4A). After being sintered at 1200 °C, a microstructure with moderate porosity and well-necked particles is formed. The average particle size and thickness of the electrode are about 5 μm and 50 μm (Fig. 4B and D), respectively. The micrograph clearly indicates that there is a good contact between the SFCN09 electrode and the CGO electrolyte. When the electrode is sintered at 1250 °C for 12 h, particle agglomeration and slightly over-sintering phenomena are observed (Fig. 4C). This effect would decrease the triple phase boundary (TPB) length and electrode porosity due to the growth of cathode particles, resulting in an increase of R_p. Similar effects had been previously reported in the literatures [18,19]. In this work, the studied electrodes were finally sintered at 1200 °C for 12 h to obtain the best sintering performance. However, the SEM images also clearly show that the porosity in the cathode is low and the particle size distribution is not uniform. Further improvement in the distribution of SFCN09 particle size and porosity in the cathode would enhance the cell performance.

Fig. 5 shows the behavior of polarization resistances as a function of temperature for the SFCN cathodes. The polarization resistance decreases with increasing the Co-doping content. This may be attributed to the increase in total electrical conductivity. On the other hand, the lower bonding energy of Co–O bond results in the loss of lattice oxygen and the formation of oxygen vacancies at elevated temperatures, a process enhanced by the Co-doping [20]. The polarization resistance of a SFCN09 cathode on CGO electrolyte is 0.74 Ω cm^2 at 750 °C. This value is similar to that of $La_{0.6}Sr_{0.4}Co_{0.8}Fe_{0.2}O_3$ for $La_{0.9}Sr_{0.1}Ga_{0.8}Mg_{0.2}O_{3-\delta}$ electrolyte IT-SOFC [21], but is still higher than those of well-known materials, such as $La_{0.6}Sr_{0.4}Co_{0.2}Fe_{0.8}O_3$ (LSCF) [22]. Hereafter, all of the electrode behavior studies are performed on SFCN09 material with CGO electrolyte.

In order to clarify the effect of oxygen partial pressure (pO_2) on the cathode process, a study of Nyquist plots at different oxygen partial pressures were carried out. Fig. 6 shows typical impedance spectra of the SFCN09/CGO cell measured at 750 °C under various oxygen partial pressures. The polarization resistance decreases dramatically with the increase of pO_2. Generally, R_p varies with the oxygen partial pressure according to the following equation [23,24]:

$$R_p = R_p^0 (pO_2)^n$$

$$n = 1, \quad O_2(g) \Leftrightarrow O_{2,ads.}$$

$$n = \tfrac{1}{2}, \quad O_{2,ads.} \Leftrightarrow 2O_{ads.}$$

$$n = \tfrac{1}{4}, \quad O_{ads.} + 2e' + V_O^{\bullet\bullet} \Leftrightarrow O_O^{\times}$$

$$n = \tfrac{3}{8}, \quad O_{TPB} + e' \Leftrightarrow O_{TPB}^{-}$$

$$n = \tfrac{1}{10}, \quad O_{TPB}^{2-} + V_O^{\bullet\bullet} \Leftrightarrow O_O^{\times}$$

The value of *n* could give useful information about the type of species involved in the reactions. The dependence of polarization resistance on oxygen partial pressure is shown in Fig. 7. The linear variation of R_p with oxygen partial pressure suggests the rate-limiting step does not significantly depend on the oxygen composition of SFCN09. Our results indicate that the *n* value is 0.23 at 750 °C, and below 750 °C, *n* values are 0.34 and 0.37 at 700 °C and 650 °C, respectively. Therefore, it is concluded that two different kinds of reaction rate-limiting steps exist on the SFCN09

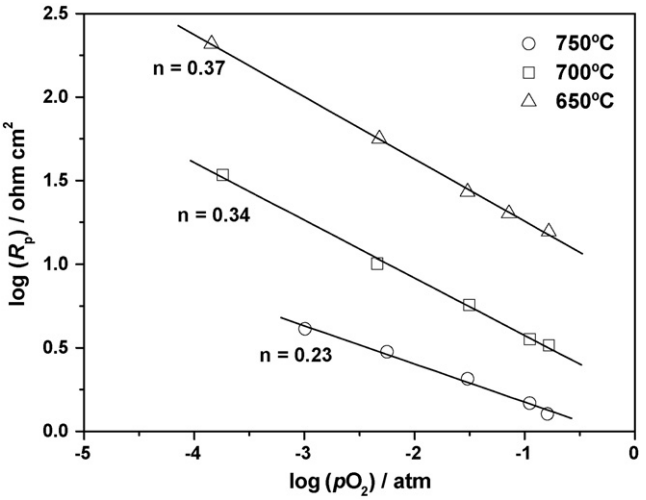

Fig. 7. Dependence of polarization resistance on oxygen partial pressure for SFCN09 cathode on CGO electrolyte at different temperatures.

electrode, depending on the temperature. With increasing temperature from 650 °C to 750 °C, the reaction rate-limiting step would be a process involving successively the oxygen ionization at triple-phase boundary (TPB) and charge transfer reaction. The complex cathode behavior observed for SFCN09 material is partially due to the easy variation of oxygen stoichiometry of this compound. The similar result has been reported before in the investigation of a $La_{0.8}Sr_{0.2}Co_{1-x}Mn_xO_{3-\delta}$ cathode [25].

Cathodic overpotential is an important parameter for SOFCs. The cathodic overpotential of SFCN09 electrode on CGO electrolyte as a function of current density at different temperatures is shown in Fig. 8. It is observed that the cathodic overpotential decreases with increasing the temperature under the same current density. When the current density reaches 88 mA cm^{-2} at 750 °C in air, the cathodic overpotential is 80 mV, which is lower than the reported Nd_2NiO_4 and $Nd_{2-x}Sr_xNiO_4$ cathode materials with perovskite-like structure [26,27]. The overpotential of SFCN09 is 81 mV at a current density of 50 mA cm^{-2} at 700 °C. At the same temperature, $Nd_{1.6}Sr_{0.4}NiO_4$ has an overpotential of about 100 mV at a current density of 50 mA cm^{-2} [27]. As we expected, the enhanced conductivity combined with some amount of oxygen vacancies formed by Co-doping in SFCN materials makes low polarization possible. Compared to the LSCF cathode material, the polarization resistance of SFCN is higher. SFCN materials are not idea for single phase SOFC cathode application because the conductivity is insufficient and could form a component in a composite cathode. Gorte reported that the electrode material should have a conductivity greater than 1 S cm^{-1} in order to be practical since a conductivity of 1 S cm^{-1} would lead to a cell resistance of 0.1 Ω cm^2 for an electrode thickness of 1 mm, even if the electrode were not porous but dense and no other loss mechanisms were operative within the electrode [1]. Therefore, the SFCN material can be considered as a promising cathode candidate for IT-SOFCs, given that the electrode performance can be further improved by optimizing the preparation of material and the microstructure of electrode, and forming composite cathodes. The previous work suggests that the performances of these cathode materials could be improved by impregnating the electrolyte and metal to enhance the conductivity and catalysis [28–30]. This work is still in process.

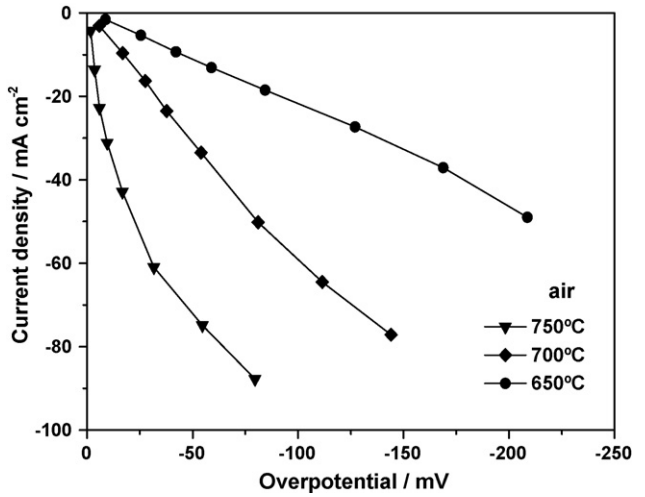

Fig. 8. The overpotential–current density curves for SFCN09 cathode on CGO electrolyte measured in air at different temperatures.

4. Conclusions

(1) The SFCN09 cathode forms a good contact with CGO electrolyte after sintering at 1200 °C for 12 h, and no reaction is observed between the SFCN09 electrode and the CGO electrolyte.
(2) The reaction rate-limiting step for oxygen reduction on the cathode depends on the temperature.
(3) SFCN09 cathode on CGO electrolyte exhibits the highest cathode performance. The lowest polarization resistance of SFCN09 is 0.74 Ω cm^2 at 750 °C in air, and the highest current density is 88 mA cm^{-2} at an overpotential of 80 mV.

Acknowledgements

This Project was supported by National Natural Science Foundation of China (Grants Nos. 20701013 and 20801016) and Research Project of Heilongjiang Educational Department (11521204) and Young Scholars of Heilongjiang University (QL200625).

References

[1] S. McIntosh, R.J. Gorte, Chem. Rev. 104 (2004) 4845–4865.
[2] S.B. Adler, Chem. Rev. 104 (2004) 4791–4843.
[3] K.C. Wincewicz, J.S. Cooper, J. Power Sources 140 (2005) 280–296.
[4] S.P. Jiang, J. Power Sources 124 (2003) 390–402.
[5] A. Petric, P. Huang, F. Tietz, Solid State Ionics 135 (2000) 719–725.
[6] H. Ullmann, N. Trofimenko, F. Tietz, D. Stöver, A. Ahmad-Khanlou, Solid State Ionics 138 (2000) 79–90.
[7] K.-I. Kobayashi, T. Kimura, H. Sawada, K. Terakura, Y. Tokura, Nature 395 (1998) 677–680.
[8] S.W. Tao, J.T.S. Irvine, J. Mater. Chem. 12 (2002) 2356–2360.
[9] Y.H. Huang, R.I. Dass, Z.L. Xing, J.B. Goodenough, Science 312 (2006) 254–257.
[10] Y.H. Huang, R.I. Dass, J.C. Denyszyn, J.B. Goodenough, J. Electrochem. Soc. 153 (2006) A1266–A1272.
[11] D. Marrero-López, J. Peña-Martínez, J.C. Ruiz-Morales, D. Pérez-Coll, M.A.G. Aranda, P. Núñez, Mater. Res. Bull. 43 (2008) 2441–2450.
[12] S.W. Tao, J. Canales-Vázquez, J.T.S. Irvine, Chem. Mater. 16 (2004) 2309–2316.
[13] T. Xia, X.D. Liu, Q. Li, J. Meng, X.Q. Cao, J. Alloy Compd. 422 (2006) 264–272.
[14] S. Zha, A. Moore, H. Abernathy, M. Liu, J. Electrochem. Soc. 151 (2004) A1128–A1133.
[15] A. Espuirol, N. Brandon, N. Bonanos, J. Kilner, M. Mogensen, B.C.H. Steele, in: A.J. Mc Evoy (Ed.), Proceedings of the Fifth European Solid Oxide Fuel Cell Forum, U. Bossel, Oberrohrdorf, Switzerland (Publ.), 2002, p. 225.
[16] N. Dasgupta, R. Krishnamoorthy, K.T. Jacob, Mater. Sci. Eng. B 90 (2002) 278–286.
[17] Y. Matsumoto, S. Yamada, T. Nishida, E. Sato, J. Electrochem. Soc. 127 (1980) 2360–2364.
[18] Y.J. Leng, S.H. Chan, Q.L. Liu, Int. J. Hydrogen Energy 33 (2008) 3808–3817.
[19] Q. Li, Y. Fan, H. Zhao, L.P. Sun, L.H. Huo, J. Power Sources 167 (2007) 64–68.
[20] K.T. Lee, A. Manthiram, J. Power Sources 158 (2006) 1202–1208.
[21] W.M. Guo, J. Liu, C. Jin, H.B. Gao, Y.H. Zhang, J. Alloys Compnd. 473 (2009) 43–47.
[22] M. Sahibzada, S.J. Benson, R.A. Rudkin, J.A. Kilner, Solid State Ionics 113–115 (1998) 285–290.
[23] Y. Takeda, R. Kanno, M. Noda, Y. Tomida, O. Yamamoto, J. Electrochem. Soc. 134 (1987) 2656–2661.
[24] E. Siebert, A. Hammouche, M. Kleitz, Electrochim. Acta 40 (1995) 1741–1753.

[25] C. Lee, S.-W. Baek, J. Bae, Solid State Ionics 179 (2008) 1465–1469.
[26] F. Mauvy, J.M. Bassat, E. Boehm, J.P. Manaud, P. Dordor, J.C. Grenier, Solid State Ionics 158 (2003) 17–28.
[27] L.P. Sun, Q. Li, H. Zhao, L.H. Huo, J.C. Grenier, J. Power Sources 183 (2008) 43–48.
[28] S.R. Wang, T. Kato, S. Nagata, T. Honda, T. Kaneko, N. Iwashita, M. Dokiya, Solid State Ionics 146 (2002) 203–210.
[29] S.P. Jiang, Mater. Sci. Eng. A 418 (2006) 199–210.
[30] W.G. Wang, M. Mogensen, Solid State Ionics 176 (2005) 457–462.